Desalination and Water Treatment 317 (2024) 100065

Contents lists available at ScienceDirect

Desalination and Water Treatment

journal homepage: www.sciencedirect.com/journal/desalination-and-water-treatment/

Magnetic recoverable $Ag_3PO_4/Fe_3O_4/\gamma$-Fe_2O_3 nanocomposite☆

Jenifer Vaswani Reboso[a,b,*], Jaime Sadhwani Alonso[a,c], Dunia E. Santiago[a,d]

[a] Universidad de Las Palmas de Gran Canaria, Escuela de Ingenierías Industriales y Civiles, Dpto. de Ingeniería de Procesos, Campus Universitario de Tafira, 35017 Las Palmas, Spain
[b] Grupo Control Analítico de Fuentes Medioambientales (CAFMA), Instituto Universitario de Estudios Ambientales y Recursos Naturales (i-UNAT), Universidad de Las Palmas de Gran Canaria, 35017 Las Palmas, Spain
[c] Grupo Sistemas Industriales de Eficiencia, Instrumentación y Protección (SEIP), Universidad de Las Palmas de Gran Canaria, 35017 Las Palmas, Spain
[d] Grupo de Fotocatálisis y Espectroscopia para Aplicaciones Medioambientales (FEAM), Departamento de Química, Instituto de Estudios Ambientales y Recursos Naturales (i-UNAT), Universidad de Las Palmas de Gran Canaria, 35017 Las Palmas, Spain

ARTICLE INFO

Keywords:
Photocatalysis
Wastewater treatment
Magnetic nanomaterials
Silver phosphate

ABSTRACT

The use of nanomaterials in water treatment is an alternative for the development of new systems to optimize the purification process. Heterogeneous photocatalysis is used for the treatment of wastewaters contaminated with recalcitrant pollutants that cannot be removed with conventional wastewater treatment techniques. Silver phosphate (Ag_3PO_4) can be used in visible-light driven photocatalysis. An important challenge of heterogeneous photocatalysis is to find a proper support for the photocatalysts to reduce the expense associated with the separation and reuse of these materials. However, the immobilization of the catalyst leads to lower reaction rates because the exposed surface area decreases and the material used as support can also interfere. In the last years, the use of magnetic materials to support photocatalysts has attracted special attention because it allows high surface areas to be exposed. Only few authors have reported the use of Ag_3PO_4/magnetic nanocomposites for photocatalysis and these need to be continued to improve their efficiency. In this work we synthesized Ag_3PO_4 and supported it on ferromagnetite (Fe_3O_4). In this study, Fe_3O_4 was synthesis following the Massart's method. Ag_3PO_4 was synthesised over Fe_3O_4 from the reaction between silver nitrate ($AgNO_3$) and disodium hydrogen phosphate (Na_2HPO_4). For characterization, DRS, SEM, XRD and magnetization studies were carried out. Ag_3PO_4 was synthesised and satisfactorily supported over magnetite ($Fe_3O_{4\text{-}23}$). The photodegradation of 10 $mg{\cdot}L^{-1}$ of methylene blue was achieved, although the apparent reaction rate constant was slightly lower for the magnetic composite than for bare Ag_3PO_4. This is explained because the composite contained 48% of the active Ag_3PO_4 material, as depicted form XRD studies.

1. Introduction

Water is a scarce resource and in many countries supply is not enough to satisfy demand. The location of water resources and their quality are factors that limit the availability of water. This problem is further complicated by climate change, rapid industrialization, population growth and the pollution of existing water resources [1]. To solve this question different solutions are proposed which include repairing water distribution infrastructures and the conservation of existing water sources. However, these options cannot increase resources. Beyond the hydrological cycle, the supply of water can only be increased by desalination and water reuse.

For this reason, a series of conventional water treatment technologies are used, which include, among others: ultraviolet radiation, chemical treatments, distillation and membrane processes (reverse osmosis, ultrafiltration, microfiltration, electrodialysis.), but all of them show specific disadvantages [2].

The continuous deterioration of the environment is a problem with greater relevance every day, and that requires short-term solutions. Most of the harmful contaminants found in natural water bodies are anthropogenic compounds that have low biodegradability and therefore cannot be removed by conventional treatments. This is the case of the so-called emerging pollutants, which are found in low concentrations in the environment and can cause ecological impacts, as well as adverse effects on health [3]. These contaminants include: drugs, additives, pesticides and a wide variety of compounds that, even at low concentrations, can alter endocrine functions [4] and increase the presence of resistant bacteria [5].

Abbreviations: SEM, scanning electron microscopy; XRD, X-ray diffraction; EDX, X-ray spectroscopy; MB, Methylene Blue

☆ Presented at the 36th International Conference on Efficiency, Cost, Optimization, Simulation and Environmental Impact of Energy Systems (ECOS 2023), 25–30 June, 2023, Las Palmas de Gran Canaria, Spain

* Corresponding author at: Universidad de Las Palmas de Gran Canaria, Escuela de Ingenierías Industriales y Civiles, Dpto. de Ingeniería de Procesos, Campus Universitario de Tafira, 35017 Las Palmas, Spain.
E-mail address: jenifer.vaswani@ulpgc.es (J.V. Reboso).

https://doi.org/10.1016/j.dwt.2024.100065
Received 14 December 2023; Received in revised form 14 December 2023; Accepted 9 January 2024

The elimination and control of these substances in aqueous media is complex due to their presence in large bodies of water. In recent years, emerging contaminants were found in practically all the studied natural water resources. For example, in Spain, more than 30 emerging contaminants were found in groundwater [6], 100 in wastewater treatment plants [7], more than 100 in the effluent of conventional wastewater treatment plants [8], several in aquaculture areas [9] and 144 in river water fish [10].

Due to the nature of these contaminants, most have proven to be poorly biodegradable, and cannot be treated in conventional wastewater treatment plants; thus, advanced oxidation processes are required to remove them [11]. Advanced oxidation processes are considered tertiary wastewater treatment techniques and can be used to eliminate compounds that are difficult to biodegrade and to reduce microbiological contamination, often with the aim of reusing the treated water. Among the most common tertiary processes we find ozonation, photocatalysis or membrane filtration.

Based on this situation and considering the development of nanotechnology, the use of nanomaterials for water treatment is an alternative that allows solving the drawbacks of traditional methods. Due to their properties, nanomaterials can contribute in obtaining stronger, lighter, cleaner and smarter surfaces and systems [12]. They have many applications ranging from automotive and aircraft (for example, reinforced and lighter materials, antifouling paints or more durable pneumatic) to biomedicine (biosensors or prosthesis).

In water treatment, nanotechnology is finding applications through different routes [13] such as the use of large surface area of nanoparticles to adsorb contaminants, the use of membranes with nanomaterials (several studies have fixed nanomaterials to different polymer membranes and have obtained a greater water flow than with conventional membranes) and the use of catalytic nanoparticles to decompose contaminants (nanomaterials have a higher photoactivity than conventional catalysts). Nanomaterials such as silver nanoparticles [14], TiO_2 nanoparticles and carbon nanotubes [15] have bactericidal effects that allow to eliminate microorganisms present in water [16]. They also have better adsorption capacities than conventional adsorbents for low concentrations of heavy metals: porous carbon nanomaterials have been used efficiently for lead, cadmium, nickel and zinc elimination [17]. Another application is to treat oils and organic solvents: SiO_2 nanoparticles fixed to a polysulfone membrane improve antifouling properties and increase permeability from 1.08 to 17.32 l/m^2·h [18]. On the other hand, boron nitride nanoslides have shown to adsorb up to 33 times their own weight in oils and organic solvents while repelling water [19]. The use of nanomaterials has also been evaluated for emerging contaminants in water treatment: a combination of titanium dioxide and graphene eliminates, under sunlight, traces of drugs and pesticides that escape from the current purification systems.

Of all the mentioned water treatment processes, we will focus on the use of nanomaterials in heterogeneous photocatalysis.

Heterogeneous photocatalysis is a relatively low-cost and sustainable technology for the treatment of many pollutants found in air and water, including organic compounds and heavy metals.

This technique is used for the treatment of wastewaters contaminated with recalcitrant pollutants that cannot be removed conventionally. One of the main drawbacks is that most photocatalysts need to be illuminated with wavelengths shorter than 388 nm [20]. However, Ag_3PO_4 has been reported to use visible light [21]. Another important challenge of heterogeneous photocatalysis is to find a proper support for the photocatalysts to reduce the expense associated with the separation and reuse of these materials. However, the immobilization of the catalyst leads to lower reaction rates because the exposed surface area decreases and the material used as support can also interfere [22]. In the last years, the use of magnetic materials to support photocatalysts has attracted special attention because it allows high surface areas to be exposed. Only few authors have reported the use of $AgPO_4$/magnetic nanocomposites for photocatalysis [21,23,24] and these need to be continued to improve their efficiency. Ag_3PO_4 is an efficient visible light driven photocatalyst that is effective in the photo-degradation of hazardous organic dyes found in contaminated wastewater [25].

In this work we synthesized Ag_3PO_4 and supported it on Fe_3O_4, performing the characterization of the synthesized material.

The aim of the study was to fabricate an Ag_3PO_4-based recoverable photocatalyst with activity under a simulated solar irradiation.

This study was developed within the framework of the research project NAPLAGUA, aimed at the application of wastewater remediation using Ag_3PO_4-based nanoparticles.

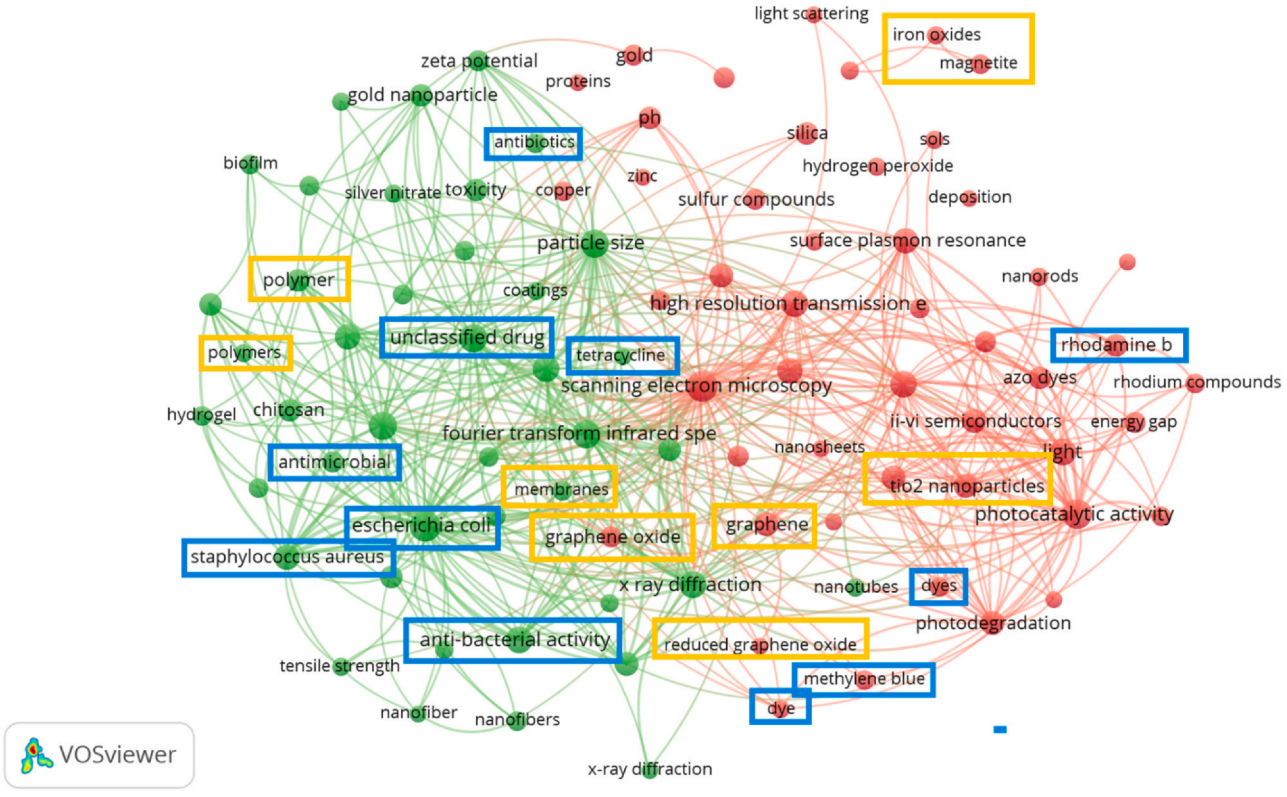

Fig. 1. Bibliometric analysis of the terms "silver nanoparticles" and "water treatment".

2. Bibliometric analysis

Bibliometric analysis is defined as a statistical evaluation of published scientific documents that enables the measure of the influence of publication in the scientific community.

The data obtained from the bibliometric analysis of the terms "silver nanoparticles" and “water treatment” are presented below. The scientific database used to search for the terms was Scopus (search conducted on May 23rd, 2021), and the software used to analyze the results was VOS Viewer®.

A growing trend was observed in the number of documents published as of 2008, with the number of documents published up to that date being less than 200. Regarding the countries with the most publications on this subject, Spain was in position number 10, with 265 publications. Among the research groups or institutions with the greatest scientific production in the field, the first Spanish institution, that is the Higher Council for Scientific Research (CSIC), was found in position number 23.

However, if we add the term “emerging pollutants” to the previous search, the number of documents is only 454 (from the year 2000 to the present). Thus, up to the year 2010, only 6 references were found in Scopus related to the study of silver nanoparticles for the treatment of emerging contaminants in water. From 2010 onwards, the number of documents begins to increase, finding in 2020, 90 documents published on this subject. In this regard, Spain was the fourth country with the most documents (27 documents in total).

Fig. 1 shows the bibliometric network resulting from the search. It is observed that the most frequently used materials for their combination with silver nanoparticles are membranes (95 occurrences), graphene oxide (192 occurrences), titanium dioxide (327 occurrences) or magnetite (122 occurrences). Regarding the final application of these materials, we mainly found keywords related to disinfection processes (*E. coli*, antibacterial activity, etc.), although words related to emerging contaminants (antibiotics, tetracycline) and dyes (blue of methylene, dyes) were also present.

3. Experimental

3.1. Sample preparation

Fe_3O_4 nanoparticles were synthesized using the Massart’s method [26–29]. Briefly, Fe_3O_4 was synthesis at pH 12 (adjusted with ammonia) by the addition of $FeCl_3$ and $FeCl_2$. The magnetic material was washed with water and dried at 80ºC.

Ag_3PO_4 was synthesized by precipitation using a NaH_2PO_4 0.15 M solution at pH 4.12 and a 0.15 M $AgNO_3$ solution. The material was then dried at 80ºC.

For the deposition of Ag_3PO_4 over the magnetic support, the synthesized Fe_3O_4 nanoparticles were dispersed in distilled water, and added to the NaH_2PO_4 solution (0.15 M, pH = 4.12). Next, the $AgNO_3$ aqueous solution (0.15 M) was added drop by drop to the above solution under continuous mechanical vibration, and then the solution was maintained at room temperature and under continuous mechanical vibration for 4 h. The magnetic material was dried at 200ºC, which enables the conversion of Fe_3O_4 into γ-Fe_2O_3, following that described in Section 4.1.

The as-prepared magnetic Ag_3PO_4 nanoparticles were separated by an external magnetic field, The final material was washed with water to remove excess phosphate and nitrate ions. The obtained magnetic Ag_3PO_4 was separated by an external magnetic field and then dried for 6 h at 80 °C.

3.2. Analysis

Powder X-ray diffraction (XRD) measurements were obtained on an X-ray diffractometer PANalytical Empyrean diffractometer (Cu Kα1, λ = 1.5406 Å). Crystallite sizes were estimated using the Scherrer equation and the fractions of the different phases were obtained from analysis with Match! 3® software.

UV–vis diffuse reflectance spectra (DRS) was measured using a Varian Cary E5 spectrophotometer in the range 200 – 2000 nm. Bandgap values were determined from the Tauc plot [30].

SEM microscopic observation allowed the visualization of the material surface morphology. For scanning electron microscopy (SEM) measurements a Sigma 300 VP FESEM Zeiss instrument was used. It was equipped with energy dispersive X-ray spectroscopy (EDX).

Magnetic measurements were carried out at 300 K using a Quantum Design MPMS XL SQUID magnetometer.

3.3. Degradation experiments

The photocatalytic activity of the synthesized materials were evaluated by the degradation of methylene blue (MB) under a simulated solar lamp. A 60 W Hapro Solarium HB175 equipped with four 15 W Philips CLEO fluorescent tubes with emission spectrum from 300 to 400 nm (maximum around 365 nm) and with an average irradiation of about 90 $W{\cdot}m^{-2}$ was used. The photocatalyst (0.1 g) was added to an aqueous solution of MB (100 mL, 10mgL^{-1}) at room temperature. The suspension was magnetically stirred for 30 min in the dark to establish an adsorption desorption equilibrium to eliminate the influence of adsorption. Next, the lamp and aeration (Turbojet 1, 72 Lh^{-1}) were switched on to initiate the reaction. During irradiation, samples were taken at different time intervals for 180 min or until complete degradation was observed. Samples were centrifuged and the concentration of MB was measured with a UV–vis spectrophotometer at 660 nm (Cary 60, Varian, USA). For comparison purposes, photolysis experiments were also carried out.

To investigate the stability and recyclability of the as-prepared composite magnetic photocatalysts ~~3434~~), recycling experiments were also performed. In the recycling experiments, after the photocatalysts were separated from the solution by an external magnetic field, the remaining solution was removed. The separated photocatalysts were washed five times with distilled water, and then used in the next degradation experiment.

The concentration of silver lixiviated from the photocatalysts was determined using inductively coupled plasma mass spectrometry ICP-MS in an external laboratory. The employed method used in the determination was based on UNE-EN ISO 17294 standard, and the detection limit was 2 $\mu g{\cdot}L^{-1}$.

The light intensity was measured with a Proskit MT-4617 digital light meter. The conversion from lux to $W{\cdot}m^{-2}$ was calculated considering that 120 lux is equivalent to 1 $W{\cdot}m^{-2}$ [31]. Results for these experiences are shown as percentage MB degradation versus accumulated energy (Ea, $J{\cdot}L^{-1}$). Ea at different time intervals was calculated following Eq. 1.

$$E_a(t) = E(t_0) + \Delta t{\cdot}\bar{G}{\cdot}\left(\frac{A}{V}\right) \quad (1)$$

where A is the area exposed to the light (that is, 0.0078 m^2), Δt is the reaction time interval, in seconds, G is the mean irradiation in the time interval, in $W{\cdot}m^{-2}$ and V is the volume of the MB solution, in L (that is, 0.1 L).

4. Results and discussion

4.1. Characterization

XRD was used to investigate the crystalline phases of the materials. Fig. 2. shows typical XRD patterns of the different samples. Fig. 2a shows the XRD pattern of Fe_3O_4 nanoparticles, Fig. 2b shows the XRD pattern of Ag_3PO_4. The successful coating and subsequent crystallization of Ag_3PO_4 over Fe_3O_4 were also confirmed (Fig. 2c).

For the Ag_3PO_4 material alone, XRD studies revealed that 100% Ag_3PO_4 was present. Similarly, for bare Fe_3O_4, 100% Fe_3O_4 was detected. For the magnetic composite, shown in Fig. 2.c, we observed the following crystalline phases: Ag_3PO_4 (47,8% ❑), magnetite (Fe_3O_4) (42,6% •) and maghemite, (γ-Fe_2O_3) (9,5% Δ). Although we initially synthesized Fe_3O_4, it is known that this structure can oxidize to γ-Fe_2O_3, also magnetic, even at ambient temperature.

The fractions of the different phases were obtained from analysis with Match! 3® software, using Chrystallography Open Database [32] [33]. Table 1 includes the identification numbers of each crystalline phase. For maghemite, the most intense peak, found at 2θ 35,86 º, corresponds to the hkl plane 311.

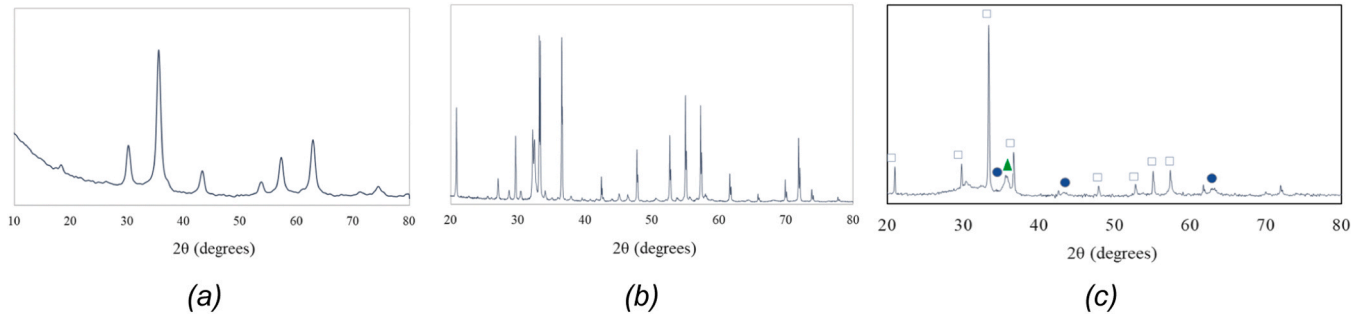

Fig. 2. XRD patterns of the samples: (a) Fe_3O_4, (b) Ag_3PO_4, (c) $Ag_3PO_4/Fe_3O_4/\gamma\text{-}Fe_2O_3$.

The calculated crystallite sizes were: 54 nm for Ag_3PO_4 and 18 nm for Fe_3O_4 and for $\gamma\text{-}Fe_2O_3$.

The formation of maghemite can occur as a consequence of the oxidation of magnetite particles, according to Eq. (2) [34]. This process can occur at room temperature [35], although it usually takes place more favourably in an oxidizing environment above 200 ºC, especially between 375 and 400 ºC [36].

$$Fe_3O_4 + ½\ O_2 \rightarrow 3\ \gamma\text{-}Fe_2O_3 \quad (2)$$

The SEM image of the three materials are ~~343423~~ shown in Fig. 3.

From Fig. 3c it is observed that there is a coating of silver phosphate on the magnetic material. Table 2 shows the elemental surface composition of $Ag_3PO_4/Fe_3O_4/\gamma\text{-}Fe_2O_3$, depicted from SEM-EDX.

UV–vis absorption spectra of the studied catalysts are shown in Fig. 4. Pure Ag_3PO_4 absorbs solar energy with a wavelength shorter than approximately 500 nm. In contrast to pure Ag_3PO_4, the absorption edge of $Ag_3PO_4/Fe_3O_4/\gamma\text{-}Fe_2O_3$ ~~3434~~ and Fe_3O_4 generates red shift: $Ag_3PO_4/Fe_3O_4/\gamma\text{-}Fe_2O_3$ ~~3434~~ and Fe_3O_4 also exhibit higher absorption in the visible region than the pure Ag_3PO_4.

The calculated bandgap (Eg) values of the different materials are shown in Table 3.

The bandgap of Ag_3PO_4 was 2.36 eV, which agrees with that reported by other authors [37,38]. The bandgap of Fe_3O_4 was the lowest (1.87 eV). This value is similar to that reported by another author for the synthesis of Fe_3O_4 at pH 10 and at room temperature (1.76 eV)[39].

The hysteresis curves of the magnetic materials are shown in Fig. 6. For magnetite and maghemite, the limit diameter from which nanoparticles present a superparamagnetic behavior is around 20 nm [40], [41]. We observed that the magnetization saturation is 43 emu·g^{-1} for Fe_3O_4 and 15 emu·g^{-1} for $Ag_3PO_4/Fe_3O_4/\gamma\text{-}Fe_2O_3$. The saturation magnetization was lower in the latter material due to the presence of Ag_3PO_4 in the shell, which reduces the magnetic contribution of the Fe_3O_4. On the other hand, $Ag_3PO_4/Fe_3O_4/\gamma\text{-}Fe_2O_3$ NPs show a relatively high saturation magnetization of 15 emu·g^{-1}, compared to that reported by other authors who employed only silver nitrate for the synthesis of magnetic Ag NPs that presented only 1 emu·g^{-1} [35].

Other authors have reported saturation magnetization ~~s~~ values around 92 emu/g for magnetite and 74 emu/g for maghemite. These numeric values are reported for massive materials of magnetite and maghemite [42].

4.2. Degradation experiment

The photocatalytic degradation of MB by ~~3434~~ $Ag_3PO_4/Fe_3O_4/\gamma\text{-}Fe_2O_3$ under simulated solar irradiation at room temperature was investigated (Fig. 5). For comparison, bare Fe_3O_4 and Ag_3PO_4 photocatalyst were also investigated. About 48% of MB was removed by ~~3434~~ $Ag_3PO_4/Fe_3O_4/\gamma\text{-}Fe_2O_3$ after 180 min irradiation. In contrast, pure Ag_3PO_4 exhibited the highest photocatalytic activity: about 96% of MB was removed within 180 min under simulated solar irradiation. Bare Fe_3O_4 did not produce the photodegradation of MB.

The apparent fist-order reaction rate constant for the degradation of methylene blue was 0.0083 min^{-1} for Ag_3PO_4 and 0.0036 min^{-1} for $Ag_3PO_4/Fe_3O_4/\gamma\text{-}Fe_2O_3$. No photolysis was observed under the studied conditions.

For Ag_3PO_4, other authors have reported an apparent reaction rate constant of 0,0036 min^{-1} and 22% degradation of a 25 mg·L^{-1} MB solution in 1 h [37]. The difference between those data and the results obtained in the present study can be attributed to the different synthesis methods employed in both studies.

Lastly, it is known that one of the mayor issues of the use of silver-based catalysts is that they can exhibit high toxicity [43]. In this sense, it has been reported that free silver ions released from the catalysts play a considerable role in the toxicity of these materials [44].

For this reason, we determined the concentration of silver in water after the photocatalytic processes when the following photocatalysts were used: bare Ag_3PO_4 and ~~3434~~ $Ag_3PO_4/Fe_3O_4/\gamma\text{-}Fe_2O_3$. We found that the lixiviation of silver was high (83.41 mg·L^{-1}) when bare Ag_3PO_4 was used. However, for ~~3434~~ $Ag_3PO_4/Fe_3O_4/\gamma\text{-}Fe_2O_3$, the release of silver was 240 µg·L^{-1}. This proves that the presence of Fe_3O_4 in the materials inhibits the release of silver to the water media. The release of silver reported in this study is much lower than that reported by other authors, which can reach up to 0.12 g·L^{-1} [45].

However further studies are needed to reduce even more the lixiviation of silver from the photocatalysts.

4.3. Separation and reuse

The recyclability of the magnetic photocatalyst was investigated. The ~~3434~~ $Ag_3PO_4/Fe_3O_4/\gamma\text{-}Fe_2O_3$ photocatalyst can be rapidly separated under an applied magnetic field in 20 s

Fig. 9 shows the recyclability of the ~~3434~~ $Ag_3PO_4/Fe_3O_4/\gamma\text{-}Fe_2O_3$ for photocatalytic degradation of MB. The degradation activity of ~~3434~~ $Ag_3PO_4/Fe_3O_4/\gamma\text{-}Fe_2O_3$ decreased sharply only after 1 cycle. The decolouration efficiency decreased to about 32%, 25%, 19% and 14% for the 2nd, 3rd,4th and 5th degradation cycles, respectively.

Efficiency decreases with reuse, and it can be observed that the catalyst darkens due to the photocorrosion of silver by irradiation. This occurs because silver phosphate is slightly soluble in water, and silver ions can react with the photogenerated electrons to form elemental silver [46].

5. Conclusions

In summary, we reported an investigation on the preparation and photocatalytic activity of a novel $Ag_3PO_4/Fe_3O_4/\gamma\text{-}Fe_2O_3$ photocatalyst.

Ag_3PO_4 was synthesised and satisfactorily supported over Fe_3O_4~~23~~. The photodegradation of 10 mg·L^{-1} of methylene blue was achieved, although the apparent reaction rate constant was slightly lower for the magnetic composite than for the Ag_3PO_4 alone. This is explained because the composite contained 47.8% of the active Ag_3PO_4 material, as depicted form XRD studies.

Photocatalytic degradative activity on blue methylene organic pollutant

Table 1
Identification numbers for XRD patterns.

Material	Identification Number
Ag_3PO_4	96-210-6405
Fe_3O_4	96-900-5842
$\gamma\text{-}Fe_2O_3$	96-900-6317

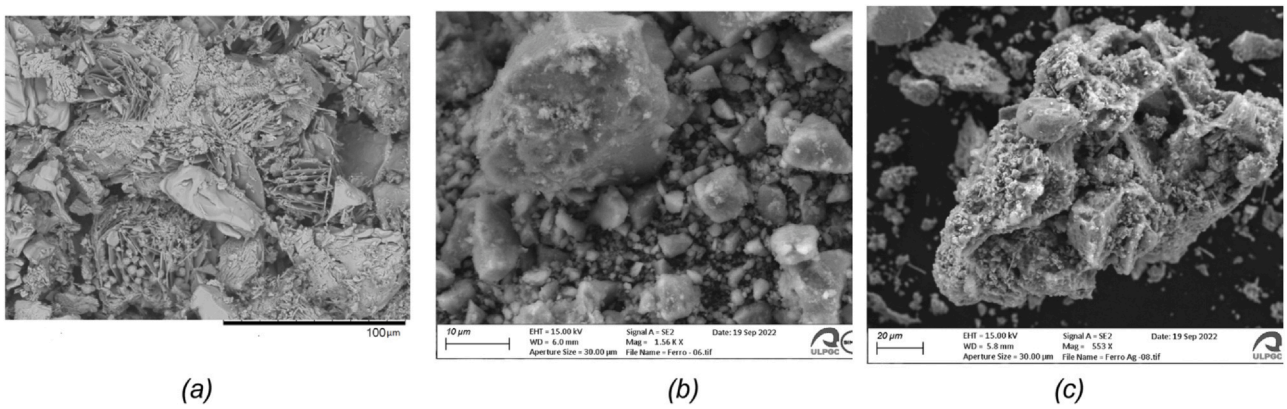

Fig. 3. SEM Images of: (a) Ag_3PO_4 (b) Fe_3O_4 (c) $Ag_3PO_4/Fe_3O_4/\gamma$-Fe_2O_3.

Table 2
Composition of Ag_3PO_4 @Fe_3O_4.

Element	Weight %	Atomic %	Error %
O K	38.97	71.81	11.71
P K	9.23	8.78	7.67
Fe K	20.63	10.89	7.56
Ag L	31.17	8.52	6.87

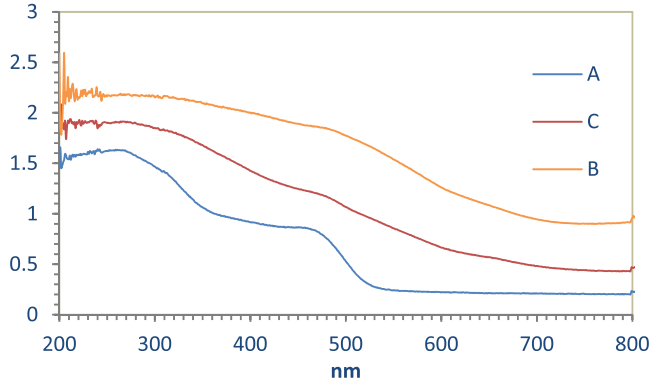

Fig. 4. UV–Vis absorption spectra of: (A) Ag_3PO_4, (B) Fe_3O_4 and (C) $Ag_3PO_4/Fe_3O_4/\gamma$-Fe_2O_3.

Table 3
Bandgap (Eg) values of the different studied materials.

Material	E_g (eV)
Ag_3PO_4	2.36
Fe_3O_4	1.87
$Ag_3PO_4/Fe_3O_4/\gamma$-Fe_2O_3	1.90

under solar simulated irradiation was studied indicating its potential use in water treatment applications.

The magnetic materials were recovered easily with a magnet. The saturation magnetization was 43 emu·g^{-1} for Fe_3O_4 and 15 emu·g^{-1} for $Ag_3PO_4/Fe_3O_4/\gamma$-Fe_2O_3. The saturation magnetization was reduced due to the presence of Ag_3PO_4 in the shell, which reduces the magnetic contribution of the Fe_3O_4.

Lastly, $Ag_3PO_4/Fe_3O_4/\gamma$-Fe_2O_3 could be reused three times with an efficiency loss of 25%. It must be noted that the material was not washed or treated between reuses. Future work must be aimed at the improvement of materials to achieve a better stability of materials for their reuse.

This study will motivate new developments in photocatalysis and promote their practical application in environmental problems.

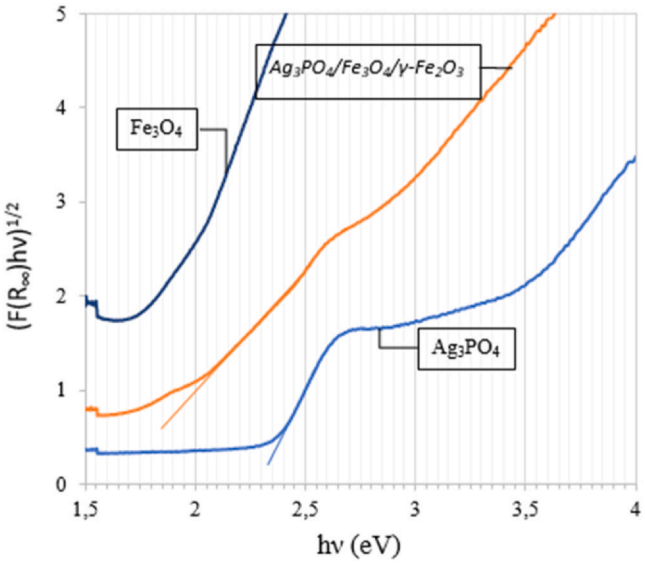

Fig. 5. Bandgap energy (E_g) determinations from the Tauc plot.

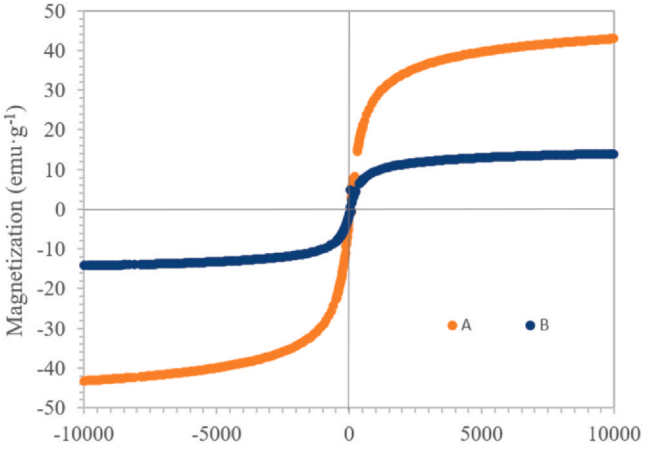

Fig. 6. Hysteresis curves of: (A) Fe_3O_4 and (B) $Ag_3PO_4/Fe_3O_4/\gamma$-Fe_2O_3.

CRediT authorship contribution statement

J. Vaswani Reboso: Conceptualization, Data curation, Investigation, Methodology, Resources, Validation, Visualization, Writing – original draft, Writing – review & editing. **Dunia E. Santiago**: Conceptualization, Data curation, Formal analysis, Investigation, Methodology, Resources, Software, Validation, Visualization, Writing – review & editing. **J. Jaime Sadhwani**

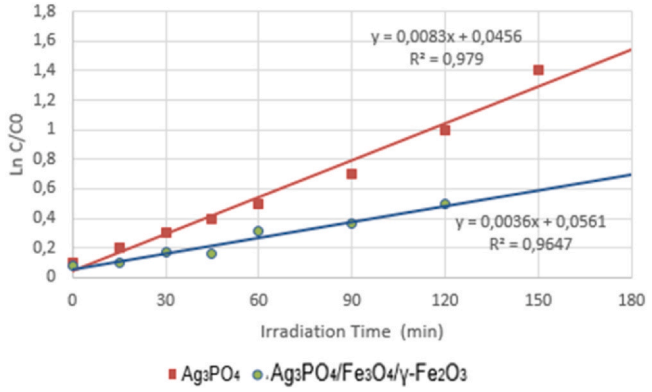

Fig. 7. Photocatalytic degradation of MB over $_{34}Ag_3PO_4$ or $Ag_3PO_4/Fe_3O_4/\gamma\text{-}Fe_2O_3$.

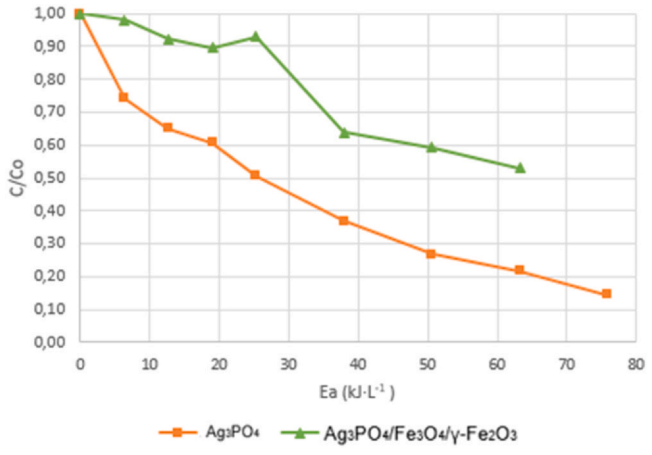

Fig. 8. Photodegradation of 10 mg·L^{-1} MB using 1 g·L^{-1} of Ag_3PO_4 or 1 g·L^{-1} of the magnetic material *$Ag_3PO_4/Fe_3O_4/\gamma\text{-}Fe_2O_3$*.

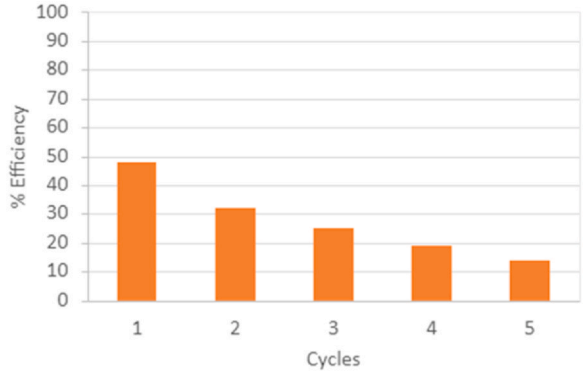

Fig. 9. Recyclability of the $Ag_3PO_4/Fe_3O_4/\gamma\text{-}Fe_2O_3$.

Alonso: Formal analysis, Funding acquisition, Project administration, Resources, Methodology, Technical research meetings, Supervision, Validation, Visualization, Review.

Declaration of Competing Interest

The authors declare that they have no known competing financial interests or personal relationships that could have appeared to influence the work reported in this paper.

Acknowledgments

This research was funded by Fundación Cajadecanarias and Fundación La Caixa through the project "Aplicación de nanopartículas a los procesos de tratamiento de aguas" (NAPLAGUA), with grant number 2021ECO14, Call for Research Projects 2021, with the collaboration of the company Ancor Tecnologica S.L. This project began in February 2022 until February 2024, with José Jaime Sadhwani Alonso as the main reseacher.

References

[1] Zaib Q, Fath H. Application of carbon nano-materials in desalination processes. Desalin Water Treat 2012;vol. 51:627–36. https://doi.org/10.1080/19443994.2012.722772.
[2] Das R, Ali ME, Hamid SBA, Ramakrishna S, Chowdhury ZZ. Carbon Nanotub Membr Water Purif: A Bright Future Water Desalin 2014.
[3] Birkholz D, Stilson SM, Elliott HS. Analysis of emerging contaminants in drinking water - a review. *Compr Water Qual Purif* 2010;vol. 2:212–29.
[4] C. García-Gómez, P. Gortáres-Moroyoqui, and P. Drogui, "Contaminantes emergentes: efectos y tratamientos de remoción," *Química Viva*, vol. 10, no. 2, pp. 96–105, Mar. 2011, [Online]. Available: ⟨https://www.redalyc.org/articulo.oa?id=86319141004⟩.
[5] M. Taheran, M. Naghdi, S.K. Brar, M. Verma, and R.Y. Surampalli, "Emerging contaminants: Here today, there tomorrow!," Environmental nanotechnology, monitoring & management, vol. v. 10. Elsevier B.V.
[6] Jurado A, Vàzquez-Suñé E, Carrera J, López de Alda M, Pujades E, Barceló D. Emerging organic contaminants in groundwater in Spain: a review of sources, recent occurrence and fate in a European context. Sci Total Environ 2012;vol. 440:82–94. https://doi.org/10.1016/j.scitotenv.2012.08.029.
[7] Bueno MJM, Gomez MJ, Herrera S, Hernando MD, Agüera A, Fernández-Alba AR. Occurrence and persistence of organic emerging contaminants and priority pollutants in five sewage treatment plants of Spain: two years pilot survey monitoring. Environ Pollut 2012;vol. 164:267–73. https://doi.org/10.1016/j.envpol.2012.01.038.
[8] Cabeza Y, Candela L, Ronen D, Teijon G. Monitoring the occurrence of emerging contaminants in treated wastewater and groundwater between 2008 and 2010. The Baix Llobregat (Barcelona, Spain). J Hazard Mater 2012;vol. 239–240:32–9. https://doi.org/10.1016/j.jhazmat.2012.07.032.
[9] Aminot Y, et al. Environ risks Assoc Contam Leg Emerg Concern Eur Aquac Areas 2019. https://doi.org/10.1016/j.envpol.2019.05.133.
[10] Pico Y, et al. Contaminants of emerging concern in freshwater fish from four Spanish Rivers. Sci Total Environ 2019;vol. 659:1186–98. https://doi.org/10.1016/j.scitotenv.2018.12.366.
[11] Gogoi A, Mazumder P, Tyagi VK, Tushara Chaminda GG, An AK, Kumar M. Occurrence and fate of emerging contaminants in water environment. " *A Rev* 2018;vol. 6:169–80. https://doi.org/10.1016/j.gsd.2017.12.009.
[12] Roduner E. Size matters: why nanomaterials are different. Chem Soc Rev 2006;vol. 35(7):583–92.
[13] Smith A. Opinion: Nanotech – the way forward for clean water? Filtr Sep 2006;vol. 43(8):32–3. https://doi.org/10.1016/S0015-1882(06)70976-4.
[14] Ahmed T, Imdad S, Yaldram K, Butt NM, Pervez A. Emerging nanotechnology-based methods for water purification: a review. Desalin Water Treat 2014;vol. 52(22–24):4089–101. https://doi.org/10.1080/19443994.2013.801789.
[15] Li Q, et al. Antimicrobial nanomaterials for water disinfection and microbial control: potential applications and implications. Water Res 2008;vol. 42(18):4591–602. https://doi.org/10.1016/j.watres.2008.08.015.
[16] M. Bodzek, K. Konieczny, and A. Kwiecińska-mydlak, "Recent advances in water and wastewater disinfection by nano-photocatalysis," vol. 305, no. December 2022, p. 29390, 2023, doi: 10.5004/dwt.2023.29390.
[17] Ruparelia JP, Duttagupta SP, Chatterjee AK, Mukherji S. Potential of carbon nanomaterials for removal of heavy metals from water. Desalination 2008;vol. 232(1):145–56. https://doi.org/10.1016/j.desal.2007.08.023.
[18] Ahmad AL, Majid MA, Ooi BS. Functionalized PSf/SiO2 nanocomposite membrane for oil-in-water emulsion separation. Desalination 2011;vol. 268(1):266–9. https://doi.org/10.1016/j.desal.2010.10.017.
[19] Lei W, Portehault D, Liu D, Qin S, Chen Y. Porous boron nitride nanosheets for effective water cleaning. Nat Commun 2013;vol. 4(1):1777. https://doi.org/10.1038/ncomms2818.
[20] Anucha CB, Altin I, Bacaksiz E, Stathopoulos VN. Titanium dioxide (TiO_2)-based photocatalyst materials activity enhancement for contaminants of emerging concern (CECs) degradation: In the light of modification strategies. Chem Eng J Adv 2022;vol. 10:100262. https://doi.org/10.1016/j.ceja.2022.100262.
[21] Guo X, et al. Performance of magnetically recoverable core–shell Fe3O4@Ag3PO4/AgCl for photocatalytic removal of methylene blue under simulated solar light. Catal Commun 2013;vol. 38:26–30. https://doi.org/10.1016/j.catcom.2013.04.010.
[22] Santiago DE, Espino-Estévez MR, González GV, Araña J, González-Díaz O, Doña-Rodríguez JM. Photocatalytic treatment of water containing imazalil using an immobilized TiO2 photoreactor. Appl Catal A Gen 2015;vol. 498:1–9. https://doi.org/10.1016/j.apcata.2015.03.021.
[23] Abroshan E, Farhadi S, Zabardasti A. Novel magnetically separable Ag3PO4/MnFe2O4 nanocomposite and its high photocatalytic degradation performance for organic dyes under solar-light irradiation. Sol Energy Mater Sol Cells 2018;vol. 178:154–63. https://doi.org/10.1016/j.solmat.2018.01.026.
[24] Liu Z, et al. The triple-component Ag3PO4-CoFe2O4-GO synthesis and visible light photocatalytic performance. Appl Surf Sci 2018;vol. 458:880–92. https://doi.org/10.1016/j.apsusc.2018.07.166.
[25] Tomar R, Abdala AA, Chaudhary RG, Singh NB. Photocatalytic degradation of dyes by nanomaterials. Mater Today Proc 2020;vol. 29:967–73. https://doi.org/10.1016/j.matpr.2020.04.144.
[26] Lv B, Xu Y, Tian H, Wu D, Sun Y. Synthesis of Fe3O4\SiO2\Ag nanoparticles and its application in surface-enhanced Raman scattering,". J Solid State Chem 2010;vol.

183(12):2968–73. https://doi.org/10.1016/j.jssc.2010.10.001.
[27] Kędzierska M, et al. The synthesis methodology of pegylated fe3o4@ag nanoparticles supported by their physicochemical evaluation. Molecules 2021;vol. 26(6). https://doi.org/10.3390/molecules26061744.
[28] Kędzierska M, et al. The Synthesis Methodology and Characterization of Nanogold-Coated Fe3 O4 Magnetic Nanoparticles. Mater (Basel) 2022;vol. 15(9). https://doi.org/10.3390/ma15093383.
[29] Dudchenko N, Pawar S, Perelshtein I, Fixler D. Magnetite Nanoparticles: Synthesis and Applications in Optics and Nanophotonics. Mater (Basel) 2022;vol. 15(7). https://doi.org/10.3390/ma15072601.
[30] Makuła P, Pacia M, Macyk W. How To Correctly Determine the Band Gap Energy of Modified Semiconductor Photocatalysts Based on UV–Vis Spectra. J Phys Chem Lett 2018;vol. 9(23):6814–7. https://doi.org/10.1021/acs.jpclett.8b02892.
[31] Michael PR, Johnston DE, Moreno W. A conversion guide: Solar irradiance and lux illuminance. J Meas Eng 2020;vol. 8(4):153–66. https://doi.org/10.21595/jme.2020.21667.
[32] N. Nakagiri, M.H. Manghnani, L.C. Ming, and S. Kimura, "Crystal structure of magnetite under pressure," *Phys. Chem. Miner.*, vol. 13, pp. 238–244, 1986, [Online]. Available: ⟨https://api.semanticscholar.org/CorpusID:96269775⟩.
[33] Pecharromán C, González-Carreño T, Iglesias JE. The infrared dielectric properties of maghemite, γ-Fe2O3, from reflectance measurement on pressed powders. Phys Chem Miner 1995;vol. 22(1):21–9. https://doi.org/10.1007/BF00202677.
[34] Laurent S, et al. Magnetic Iron Oxide Nanoparticles: Synthesis, Stabilization, Vectorization, Physicochemical Characterizations, and Biological Applications. Chem Rev 2008;vol. 108(6):2064–110. https://doi.org/10.1021/cr068445e.
[35] Haneda A, Morrish K. Magnetite to maghemite transformation in utrafine particles.,". J Phys Colloq 1977;vol. 38:321–3. https://doi.org/10.1051/jphyscol:1977166.
[36] Lepp H. "Stages in the oxidation of magnetite,". Am Mineral 1957;vol. 42:679–81.
[37] Liu JJ, Fu XL, Chen SF, Zhu YF. Electronic structure and optical properties of Ag3PO4 photocatalyst calculated by hybrid density functional method. Appl Phys Lett 2011;vol. 99(19):191903. https://doi.org/10.1063/1.3660319.
[38] Yu C, et al. Ag(3)PO(4)-based photocatalysts and their application in organic-polluted wastewater treatment.,". Environ Sci Pollut Res Int 2022;vol. 29(13):18423–39. https://doi.org/10.1007/s11356-022-18591-7.
[39] Saragi T, Depi BL, Butarbutar S, Permana B, Risdiana. The impact of synthesis temperature on magnetite nanoparticles size synthesized by co-precipitation method. J Phys Conf Ser 2018;vol. 1013(1):0–4. https://doi.org/10.1088/1742-6596/1013/1/012190.
[40] Teja AS, Koh PY. Synthesis, properties, and applications of magnetic iron oxide nanoparticles. Prog Cryst Growth Charact Mater 2009;vol. 55(1–2):22–45. https://doi.org/10.1016/j.pcrysgrow.2008.08.003.
[41] Chatterjee J, Haik Y, Chen CJ. Size dependent magnetic properties of iron oxide nanoparticles. J Magn Magn Mater 2003;vol. 257(1):113–8. https://doi.org/10.1016/S0304-8853(02)01066-1.
[42] Ho DON, Sun X, Sun S. Theranostic Applications. Acc Chem Res 2011;vol. 44(10):875–82.
[43] Tortella GR, et al. Silver nanoparticles: Toxicity in model organisms as an overview of its hazard for human health and the environment. J Hazard Mater 2020;vol. 390:121974. https://doi.org/10.1016/j.jhazmat.2019.121974.
[44] Beer C, Foldbjerg R, Hayashi Y, Sutherland DS, Autrup H. Toxicity of silver nanoparticles—Nanoparticle or silver ion? Toxicol Lett 2012;vol. 208(3):286–92. https://doi.org/10.1016/j.toxlet.2011.11.002.
[45] Xu J-W, Gao Z-D, Han K, Liu Y, Song Y-Y. Synthesis of Magnetically Separable Ag3PO4/TiO2/Fe3O4 Heterostructure with Enhanced Photocatalytic Performance under Visible Light for Photoinactivation of Bacteria. ACS Appl Mater Interfaces 2014;vol. 6(17):15122–31. https://doi.org/10.1021/am5032727.
[46] Chen X, Dai Y, Wang X. Methods and mechanism for improvement of photocatalytic activity and stability of Ag3PO4: A review. J Alloy Compd 2015;vol. 649(C):910–32. https://doi.org/10.1016/j.jallcom.2015.07.174.